

RSC Advances

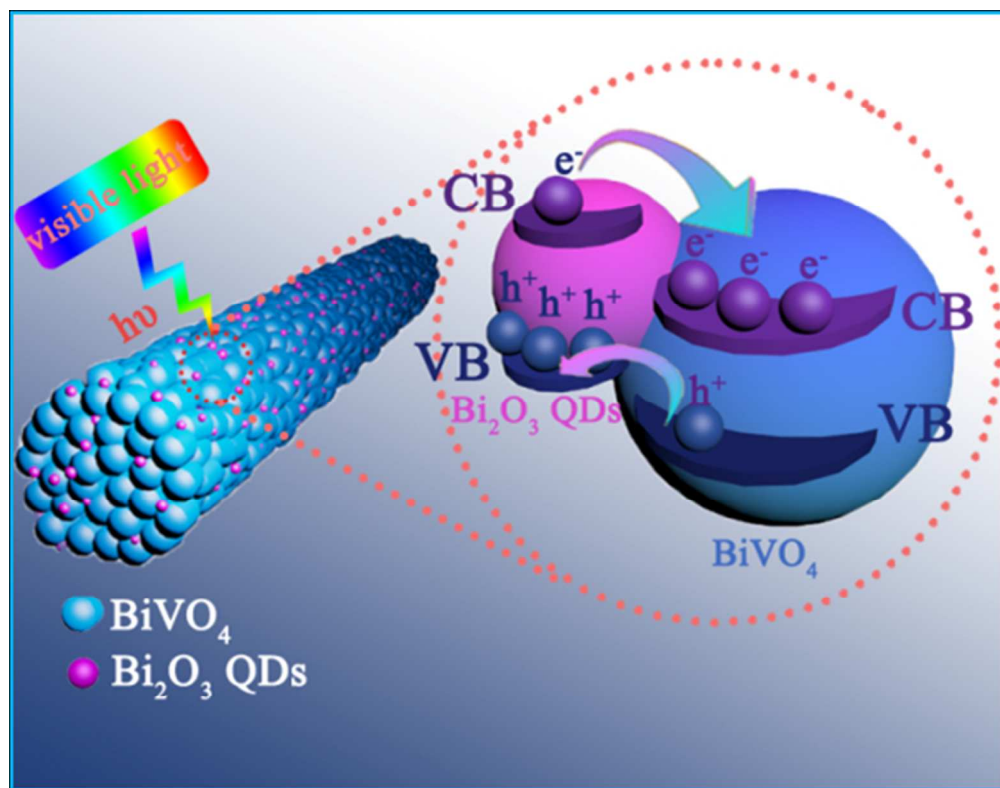


This is an *Accepted Manuscript*, which has been through the Royal Society of Chemistry peer review process and has been accepted for publication.

Accepted Manuscripts are published online shortly after acceptance, before technical editing, formatting and proof reading. Using this free service, authors can make their results available to the community, in citable form, before we publish the edited article. This *Accepted Manuscript* will be replaced by the edited, formatted and paginated article as soon as this is available.

You can find more information about *Accepted Manuscripts* in the [Information for Authors](#).

Please note that technical editing may introduce minor changes to the text and/or graphics, which may alter content. The journal's standard [Terms & Conditions](#) and the [Ethical guidelines](#) still apply. In no event shall the Royal Society of Chemistry be held responsible for any errors or omissions in this *Accepted Manuscript* or any consequences arising from the use of any information it contains.



137x107mm (111 x 111 DPI)

Cite this: DOI: 10.1039/c0xx00000x

www.rsc.org/xxxxxx

ARTICLE

One-dimensional Bi₂O₃ QDs decorated BiVO₄ nanofibers: electrospinning synthesis, phase separation mechanism and enhanced photocatalytic performance†

Chade Lv, Gang Chen*, Jingxue Sun*, Chunshuang Yan, Hongjun Dong and Chunmei Li

Received (in XXX, XXX) Xth XXXXXXXXX 20XX, Accepted Xth XXXXXXXXX 20XX
DOI: 10.1039/b000000x

Abstract: In this work, we design and successfully fabricate a novel Bi₂O₃ quantum dots (QDs) decorated BiVO₄ nanofibers by a direct heat treatment of as-spun fibers. The Bi₂O₃ quantum dots with a size of 5-15 nm are well dispersed on the surface of the BiVO₄ nanofibers with a diameter of 400-700 nm to form a Bi₂O₃ QDs decorated BiVO₄ nanofibers photocatalyst. Based on the phase separation mechanism and the properties of solvents, a possible formation process of the Bi₂O₃ QDs decorated BiVO₄ nanofibers has been proposed. The BiVO₄ nanofibers with the decoration of Bi₂O₃ QDs exhibit much better photocatalytic performance than pure BiVO₄ nanofibers. Photocurrent responses and electrochemical impedance spectra prove that decorating BiVO₄ nanofibers with tiny size Bi₂O₃ QDs can effectively promote the separation of photoinduced carriers, which is benefit for photocatalytic properties. More significantly, this work is avail to environmental purification and photoelectrochemical.

1 Introduction

In morden society, the application of semiconductor photocatalysts to solar energy converse and environment purification have attracted extensive attention.^{1, 2} Nowadays, owing to their specific crystalline structure, a lot of progress of bismuth-based photocatalysts have been achieved, such as BiOX (X = Cl, Br, I)^{3, 4}, BiVO₄⁵, Bi₂MoO₆⁶, Bi₂O₃^{7, 8}, Bi₄Ti₃O₁₂⁹ and Bi₂WO₆^{10, 11}.

Among them, BiVO₄ ($E_g \approx 2.40\text{eV}$) has been found to be an outstanding visible-light-response photocatalyst for pollutants degradation and oxygen evolution owing to its particular structure of the valence band (formed by Bi 6s or a hybrid orbital of Bi 6s and O 2p) and the conduction band (formed by V 3d).¹²⁻¹⁶ However, it impedes the practical application of BiVO₄ in environment decontamination that there exists shortcoming in effectively separating photoactivated electron-hole.^{15, 16} As a result, great effort has been made to improve its photocatalytic properties *via* building heterojunction,¹⁷ morphological controlling,¹⁸ ion doping,¹⁹ facet selective deposition,²⁰ and so on. In addition, surface modification or decoration has also been widely used to enhance the photocatalytic performance because surface modification and decoration may have significant influence on the photocatalytic process by altering the charge-transfer pathways occurring at the water-photocatalysts interface and light absorption property of photocatalysts.^{21, 22} For instance, gold particles have been decorated on the surface of BiVO₄ nanotubes and nanosheets forming a Au/BiVO₄ heterogeneous

nanostructures, thus the photocatalytic activity is markedly enhanced due to the surface plasma resonance effect.²³ Besides, surface fluorination not only affects surface or bulk incorporation of fluorine as the post-fluorination (exposure of pre-crystallized photocatalyst to fluorine-containing atmosphere), but also is highly flexible in controlling the crystal modification in terms of phase, size, crystallinity, shape and exposed crystal facets which are responsible for photocatalytic activity.²⁴

Recently, as a novel method among many surface modification skills, semiconductor quantum dots have been widely used to decorate photocatalysts by surface loading or embedding, such as CdS QDs/TiO₂, CdTe QDs/ZnO and Bi₂S₃ QDs/TiO₂.²⁵⁻²⁷ Constructing a surface decoration system which contains semiconductor quantum dots and substrate photocatalysts can effectively improve the photocatalytic properties due to the high surface-to-volume ratio of quantum dots and the promotion of charge carriers separation.²⁸ However, the quantum dots aggregate easily to minimize the specific area caused by the high surface energy, that will contribute to adverse effect on photocatalysis. Until now, to handle with above problem, only a few methods have been taken to fabricate quantum dots decorated photocatalysts, including hydrothermal method, refluxing, pyrolysis of the organometallic precursors, ultrasonic method, and so on.²⁸⁻³¹ Nevertheless, electrospinning can solve the problem more perfectly because electrospinning is a facile preparation method to fabricate photocatalysts with stable structure and large specific area for preventing quantum dots from aggregation. The quantum dots can well dispersed on/into the one-dimensional (1D) photocatalysts to form composite

photocatalysts.³²⁻³⁴ In addition, electrospinning is an ideal technique to yield abundant amounts of continuous nanofibers with 1D structure. The fibers are porous and the diameter can be controlled in a range of nanometers to a few micrometers.^{35, 36}

Therefore, electrospun quantum dots/nanofibers composite photocatalysts has been fabricated with excellent photocatalytic activity.²¹ However, to the best of our knowledge, the quantum dots decorated BiVO₄ nanofibers fabricated by electrospinning have not been reported.

Among many quantum dots candidates to decorate BiVO₄ fibers, bismuth-based photocatalyst, Bi₂O₃ which possess a feasible bandgap ($E_g \approx 2.8$ eV) is an ideal choice to construct heterojunction with BiVO₄.^{37, 38} Up to now, Bi₂O₃ quantum dots have been prepared to enhance the photocatalytic performance of TiO₂ and Bi₃NbO₇ semiconductor photocatalysts by fabricating composite photocatalysts.^{39, 40}

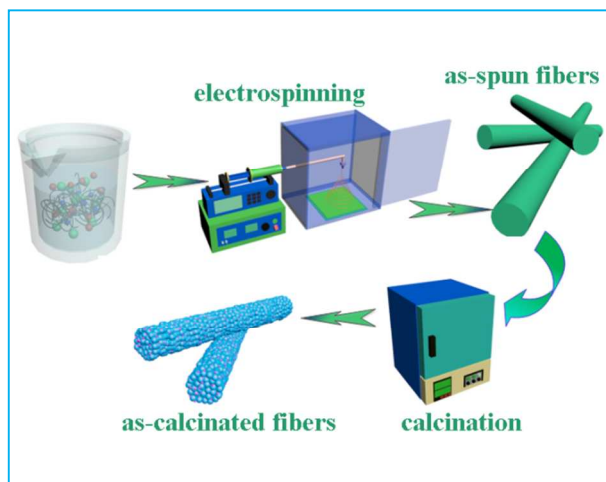
Herein, we demonstrate the *in situ* synthesis of Bi₂O₃ quantum dots decorated BiVO₄ nanofibers *via* a facile electrospinning method. As a comparison, BiVO₄ nanofibers are prepared under a similar condition, where the solvents proportion is the only variable. A reasonable formation process is put forward based on the solvents properties and phase separation mechanism. The as-prepared Bi₂O₃ QDs decorated BiVO₄ nanofibers exhibit a much higher visible-light-driven photocatalytic activity than BiVO₄ nanofibers. Besides, it could direct the industrial production of efficient photocatalysts by electrospinning in the future.

2 Experimental

2.1 Preparation of Catalysts

All reagents were of analytical purity, received from Aladdin reagents (Shanghai) company, and used without further purification. In a typical synthesis, 0.84 g of citric acid was dissolved in 6 mL of ethanol with magnetic stirring at room temperature, and then 0.6468 g of Bi(NO₃)₃·5H₂O was added into the mixture. After the Bi(NO₃)₃·5H₂O dissolved, 0.1560 g NH₄VO₃ was added slowly into the Bi(NO₃)₃ solution. Afterward, the above mixture was joined into a certain concentration of PVP (poly(vinylpyrrolidone), K-90) DMF (N,N-Dimethylformamide) solution (2.0 g of PVP was dissolved in 20 mL of DMF) with continuous stirring 12 h. Thus the spinnable precursor sols were obtained. Then, the precursor sols were transferred into a 10 mL syringe which was attached to a stainless steel needle with inner diameter of 0.510 mm (21 G) and then were ejected from the needle with a voltage of 14 kV. The distance between the needle and collector was 12 cm. And the feeding rate of the suspension in the syringe is controlled as 1.0 mL·h⁻¹ by using a syringe pump. The sols were spun at about 25 °C in air by electricity. The humidity was controlled below 30%. The as-spun fibers in the form of nonwoven mats were collected from a collector plate (Al foil). The as-spun fibers were annealed at 500 °C for 2 h with a ramp rate of 1 °C min⁻¹ using a chamber furnace. The scheme of electrospinning process was shown in Scheme 1. The calcination samples were Bi₂O₃ quantum dots decorated BiVO₄ nanofibers (denoted as BQDs-BVNFs). As a contrast, the BiVO₄ nanofibers were fabricated by a similar route. The only change of the synthesis condition was the solvents proportion which was adjusted to 16 mL DMF and 10 mL

ethanol. The as-calcinated



Scheme. 1 Scheme diagram of fabrication of BQDs-BVNFs.

60 samples were pure BiVO₄ nanofibers (denoted as BVNFs).

2.2 Characterization

The structure of the obtained monoclinic scheelite BiVO₄ was confirmed by X-ray diffraction (XRD) on Rigaku D/max-2000 diffractometer with Cu K α radiation ($\lambda = 0.15406$ nm). Diffraction patterns were collected from 10 ° to 90 ° at a speed of 4 °/min with a scan width of 0.02 °. The morphology of the products was observed by a Camscan MX2600FE field emission scanning electron microscope (FE-SEM). The operating voltage was set to 20 kV and the sample was prepared by dropping the pre-ultrasonic-dispersed (10 min) ethanol turbid liquid onto the chip of silicon. Transmission electron microscopy (TEM) and high-resolution TEM (HRTEM) of the hierarchical structures were carried out on FEI Tecnai G2 S-Twin operating at 300 kV. UV-vis diffuse reflectance spectra were acquired by a spectrophotometer (TU-1900) and BaSO₄ was used as the reflectance standard. Raman spectra were recorded on a HORIBA Xplore instrument with an Ar⁺ laser source of 488 nm wavelength in a macroscopic configuration (532 nm). X-ray photoelectron spectroscopy (XPS) analysis was measured on an American electronics physical HI5700ESCA system with X-ray photoelectron spectroscope using Al K α (1486.6 eV) monochromatic X-ray radiation. The peak positions were corrected against the C 1s peak (284.6 eV) of contaminated carbon.

2.3 Photocatalytic Test

The photocatalytic activities of the samples were evaluated by the degradation of RhB under simulated sunlight irradiation by using a 300 W Xe lamp (Trusttech PLS-SXE 300, Beijing) with a cutoff filter ($\lambda \geq 400$ nm). The RhB initial concentration was 10 mg/L. A 0.05 g amount of photocatalysts was put into 100 mL of RhB solution. Before the photodegradation experiment was initiated, the suspension was magnetically stirred in the dark for 55 min to reach adsorption-desorption equilibrium and sonicated for 5 min. The final preparation was the addition of 0.1 mL H₂O₂ into the above solution. Once the photodegradation experiment started, at given time intervals, 4 mL aliquots solution were

sampled and centrifuged to remove the photocatalysts. The filtrates were analyzed by the variations of the absorption-band maximum (554 nm). The photodegradation efficiency of the RhB was estimated according to the following formula: $\eta = [(A_0 - A_t)/A_0] * 100\%$, where A_0 and A_t are the absorbance of the pre- and postirradiation of the RhB solution, respectively. For photocatalytic activity comparison, the BiVO_4 nanofibers with a glossy surface were synthesized *via* the same condition except the proportion of solvents (DMF: 16 mL, ethanol: 10 mL).

2.4 Photoelectrochemical measurements

The photoelectrochemical characteristics were measured in a CHI604C electrochemical working station using a standard three-compartment cell. Catalyst coated FTO glass served as working electrode and a piece of Pt sheet, a Ag/AgCl electrode and 0.5 M sodium sulfate were used as the, counter electrode, reference electrode and electrolyte, respectively. The photocurrent and the electrochemical impedance spectroscopies (EIS) were carried out at the open circuit potential. The light source employed was a 300 W xenon light source.

3 Results and discussion

Fig. 1 shows the XRD patterns of BQDs-BVNFs and BVNFs synthesized by electrospinning and subsequent annealing treatment at 500 °C for 2 h. The XRD patterns of these two samples are assigned to monoclinic scheelite BiVO_4 which is in good agreement with the standard card of No. 14-0688. From the observation of the XRD pattern, with the decoration of Bi_2O_3 quantum dots on the BiVO_4 , there is no obvious shift of main peaks of BiVO_4 , demonstrating that the Bi species are present in a separate phase rather than incorporated into the BiVO_4 lattice, which is similar to previous results.^{39,41} However, no characteristic peaks belonging to Bi_2O_3 QDs are found in the BQDs-BVNFs. The absence of XRD peaks of Bi_2O_3 QDs is ascribed to their very small size and low content in BVNFs.^{31,42,43}

The SEM and TEM images of as-spun fibers and the BQDs-BVNFs are shown in Fig. 2. As Fig. 2a shows, the as-spun fibers are one-dimensional uniform texture structure with a glossy surface and randomly oriented under this synthesis condition (DMF : ethanol = 20 mL : 6 mL). The diameter of these as-spun fibers is about 100-300 nm, and the length of individual fibers is up to tens of micrometers. After calcination at 500 °C, the surface

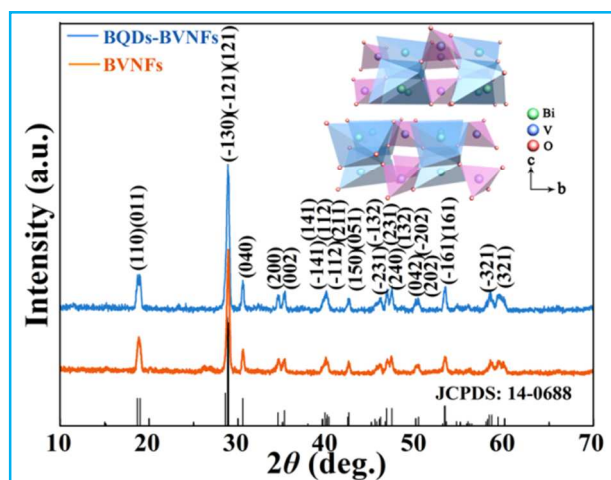


Fig. 1 The XRD patterns of the BQDs-BVNFs and BVNFs.

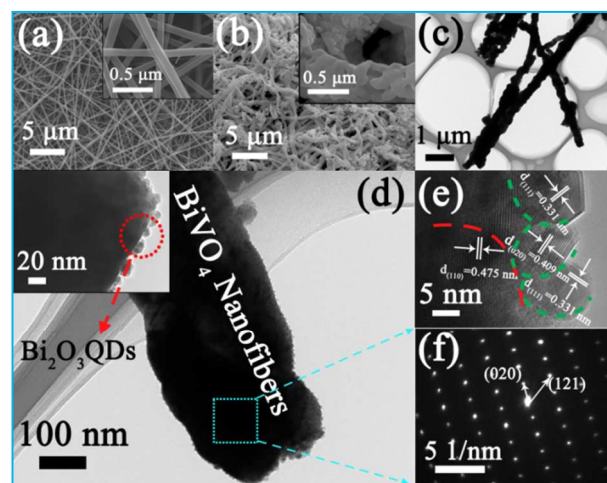


Fig. 2 (a, b) SEM images of the as-spun fibers and BQDs-BVNFs; the inset is at high magnification. (c,d) TEM images of the BQDs-BVNFs at low magnification; the inset in (d) is the local surface at the high magnification. (e) HRTEM image of the BQDs-BVNFs. (f) The corresponding selected area electron diffraction pattern.

of the BQDs-BVNFs is much coarser due to decomposition of organic ingredient and redundant ions, but the fibers can still retain the one-dimensional structure. Meanwhile, the diameter of BQDs-BVNFs (300-600 nm) exhibits a dissimilar result that it is larger than that of as-spun fibers. The unique phenomenon may result from the surface element gathering of as-spun fibers, which is proved in below XPS spectra. Further information about the BQDs-BVNFs one-dimensional structure is obtained from TEM images (Fig. 2c-f). It is confirmed that nanofibers have diameters of about 300-600 nm, which agrees well with that revealed by SEM images. The QDs in 5-15 nm are well dispersed on the surface of the BiVO_4 nanofibers as shown in Fig. 2d. The HRTEM investigation demonstrates the nanofibers are composed of the BiVO_4 nanoparticles and the interplanar spacing is 0.475 nm, which corresponds well to the (110) plane of monoclinic BiVO_4 . Besides, the Bi_2O_3 quantum dots with a diameter of 5-15 nm can be observed on the surface of the BiVO_4 nanofibers and the interplanar spacings of 0.331 nm and 0.409 nm correspond to the (111) and (020) plane of $\alpha\text{-Bi}_2\text{O}_3$, respectively. The legible diffraction spots of the corresponding SAED pattern can be indexed as the (020) and (121) reflections (Fig. 2f), demonstrating the centre of BiVO_4 nanofibers consist of BiVO_4 nanocrystals. As shown in Fig. S1,[†] SAED pattern of the fibers' surface could confirm the existence of $\alpha\text{-Bi}_2\text{O}_3$ on the surface. Furthermore, the SAED patterns selected from different region (centre or surface) exhibit different diffraction pattern, indicating the Bi_2O_3 QDs are attached to the surface of BiVO_4 nanofibers.

As Fig. 3 shows, when changing the proportion of the solvents (DMF : ethanol = 8 : 5) with keeping other conditions invariable, the morphology of the as-prepared sample changes observably. The as-spun fibers of BVNFs are similar to that of the BQDs-BVNFs in diameter and length as shown in Fig. 3a. However, many branch-like fibers appear due to the elongating viscoelastic thread stress balance which are caused by the change of variation of solvents proportion.⁴⁴ Fig. 3b shows that the BiVO_4 nanofibers still maintain the one-dimensional structure after the heat

treatment, and the diameter of BVNFs is 200-500 nm. Besides, as observed in Fig. 3c, the surface of the as-prepared BiVO_4

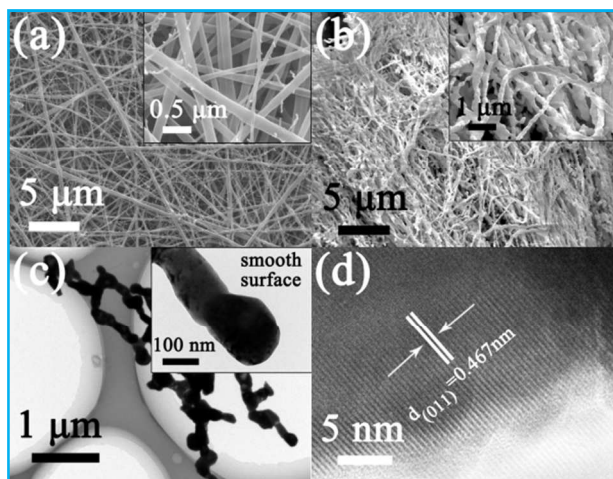


Fig. 3 (a, b) SEM images of the as-spun fibers and BVNFs; the inset is at high magnification. (c) TEM image of the BVNFs at low magnification; the inset is at high magnification. (d) HRTEM image of the BVNFs.

nanofibers is smooth and no Bi_2O_3 QDs could be observed in the inset image. The HRTEM images illustrated in Fig. 3d indicate the interlinked nanoparticles of the smooth BiVO_4 nanofibers are single crystalline and the interplanar spacing is 0.467 nm, which corresponds well to the (011) plane of monoclinic BiVO_4 .

To investigate the effect of the formation of Bi_2O_3 quantum dots on BiVO_4 nanofibers, the local structures of BQDs-BVNFs and BVNFs are studied by Raman spectroscopy. Fig. 4 shows the Raman spectra of BQDs-BVNFs and BVNFs excited by a green-line laser (532 nm). As Fig. 4a shows, Raman bands around 210, 324, 366, 710, and 826 cm^{-1} are observed in both two samples. These are ascribed to the typical vibrational bands of BiVO_4 .^{24, 45, 46} The band located at 210 cm^{-1} is the external mode of BiVO_4 , which offers negligible structural information. The Raman bands at 324 and 366 cm^{-1} are attributed to the asymmetric and symmetric deformation modes of the VO_4^{3-} tetrahedron, respectively.⁴⁵ The Raman bands around 710 and 826 cm^{-1} are assigned to the stretching modes of two different types of V-O bonds. In addition, an obvious Raman band shift of the V-O stretching vibration is observed, which is owing to the one-dimensional structural BiVO_4 nanofibers.⁴⁷ From observation in Fig. 4b, which is the magnified spectrum corresponding to the red dotted line circle part in Fig. 4a, there exists a small peak around 461 cm^{-1} of BQDs-BVNFs, whereas there is no peak at the same position of BVNFs. This additional Raman band of BQDs-BVNFs is ascribed to the Bi_2O_3 quantum dots decorated on the surface of the BiVO_4 nanofibers.⁴⁸

Considering that heating treatment process of BQDs-BVNFs is

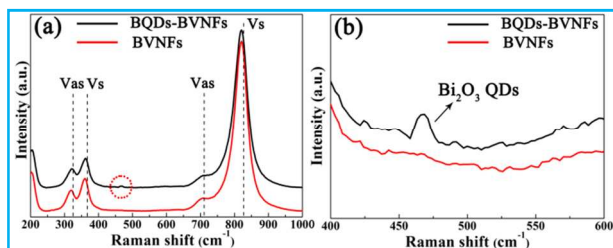


Fig. 4 Raman spectra of BQDs-BVNFs and BVNFs excited by a green-line laser (532 nm): (a) characteristic peaks of BiVO_4 nanofibers lie in the region of 200-1000 cm^{-1} . (b) the magnifying region of 400-600 cm^{-1} .

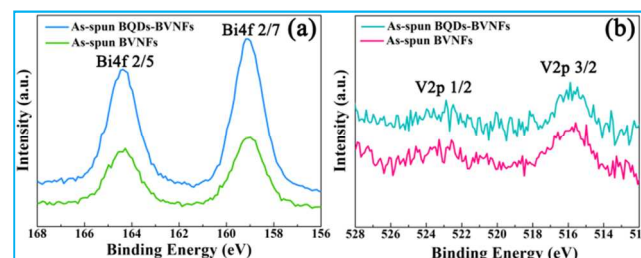


Fig. 5 XPS spectra of the as-spun fibers of both two samples: (a) the Bi 4f and (b) V 2p peak.

consistent with that of BVNFs, the formation of Bi_2O_3 quantum dots surface decorated BiVO_4 nanofibers could attribute to the difference in surface chemical composition of the as-spun fibers between the as-spun fibers of two samples. Therefore, the XPS has been taken to investigate the distribution of surface element in as-spun fibers of BQDs-BVNFs and BVNFs.⁴⁹ Fig. 5 shows the characteristic spin-orbit split peaks of the Bi 4f 5/2 and Bi 4f 7/2 signals, V 2p 1/2 and V 2p 3/2 signals. The peak positions of both Bi and V in the two as-spun fibers are both close to the BiVO_4 reported in other study.²⁴ However, owing to the existence of the organic component (PVP and citric acid) which possess a coordination capacity to complex with Bi^{3+} and V^{5+} , thus, the electron density increases and both of the spin-orbit split peaks shift towards the lower binding energy region. Furthermore, as shown in Fig. 5a, the Bi 4f 5/2 and Bi 4f 7/2 signal peaks of the as-spun BQDs-BVNFs are much stronger than that of as-spun BVNFs. On the contrary, the V 2p 1/2 and V 2p 3/2 signal peaks of two samples shown in Fig. 5b exhibit a nearly accordant intensity. From the observation, the summing-up could be put forward that there exists surface element gathering in as-spun fibers of BQDs-BVNFs.

Based upon the synthesis condition and above analysis results, a possible formation mechanism of BQDs-BVNFs is described in Fig. 6. In the procedure of the precursor solution preparation, bismuth(III) nitrate pentahydrate first dissolved in citric acid solution. The addition of citric acid to the solution not only provide an acidic condition which can effectively inhibit the hydrolysis of Bi^{3+} ions, but also leads to a complexing reaction with Bi^{3+} ions. Ammonium metavanadate powder is added slowly into the above solution and a blue green homogeneous liquid

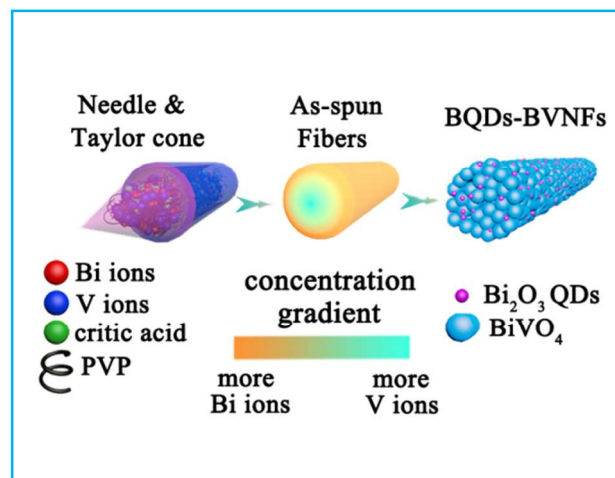


Fig. 6 Possible formation process of Bi_2O_3 quantum dots decorated BiVO_4 nanofibers.

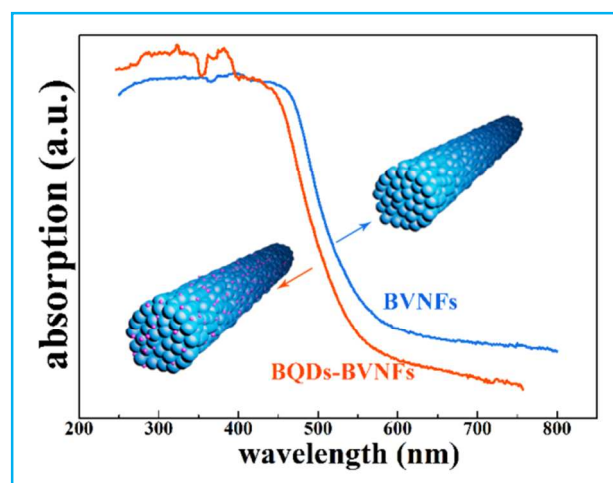


Fig. 7 The UV-vis diffuse reflectance spectra of the BQDs-BVNFs and BVNFs samples.

forms because of the valence change of the vanadium. In the precursor solution, each ingredient is well-distributed under the vigorous stirring. However, it is different in the surface tension and conductivity between DMF and ethanol which can influence the formation of the fibers.^{50,51} As the surface tension of DMF is smaller than that of ethanol, nevertheless, the conductivity is much larger, the Taylor cone which contains more DMF will take shape easily.⁵² In addition, Bi^{3+} ions are most likely dissolved in DMF. On the contrary, vanadate ions prefer to ethanol. Given that we have given greater volume to the DMF in this system (DMF : ethanol = 10 : 3), a concentration gradient of solvents could come into being naturally, as the Fig. 6 shows. Therefore, the Bi^{3+} ions diffuse to the shell level while the vanadate ions diffuse to the core level. Afterwards, the Bi^{3+} ions in the shell level could contribute to the evolution of the Bi_2O_3 quantum dots because they are easily exposed to the air atmosphere and react with O_2 instead of reacting with vanadate ions in the process of calcination. However, the characteristic peaks of BQDs-BVNFs do not shift shown in XRD pattern, indicating that extra V ions could not lead to the formation of non-stoichiometric BiVO_4 . Nevertheless, when changing the proportion of the solvents (DMF : ethanol = 8 : 5), the concentration gradient of solvents is

not obvious any more. As a result, each composition is well-

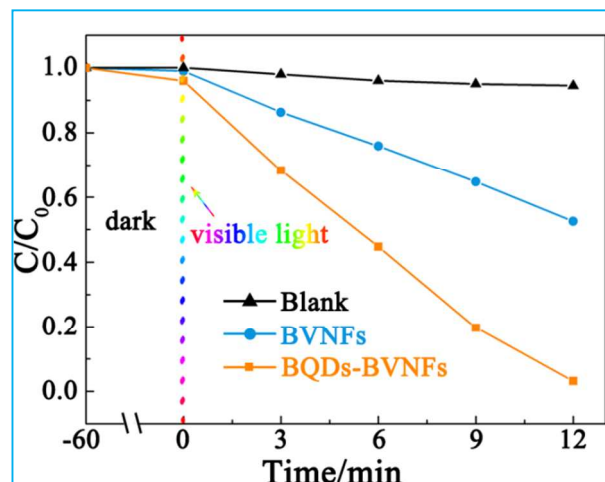


Fig. 8 Photocatalytic degradation of RhB under visible-light irradiation.

dispersed in the as-spun fibers, which lead to the formation of smooth BiVO_4 nanofibers without BQDs decoration.

UV-visible diffuse reflectance spectroscopy (DRS) is used to characterize the light absorption property of the as-prepared samples. Fig. 7 shows the UV-visible absorption spectra of BQDs-BVNFs and BVNFs samples. Both of the samples possess the ability to utilize the visible light for photocatalysis due to their absorption edge located at ca. 550 nm as shown in the spectra. Besides, as observed from the plot, there is no shoulder peak, which concludes that impurity level doesn't generate with the decoration of Bi_2O_3 quantum dots. The accordant deduction has been proposed from XRD analysis above. However, BQDs-BVNFs exhibit an obvious blue shift because of the existence of the Bi_2O_3 QDs, of which the bandgap is wider than that of BiVO_4 .

The photocatalytic activities of the products are evaluated by the decomposition of RhB under visible light ($\lambda \geq 400$ nm). Fig. 8 shows the photocatalytic degradation rate of BQDs-BVNFs and BVNFs under visible-light irradiation. Without the addition of the photocatalysts (blank), there is no obvious decrease of the C (the absorption of RhB at 554 nm). However, after the addition of photocatalysts, the C declined drastically, and the BQDs-BVNFs exhibit a higher photocatalytic performance than the BVNFs photocatalysts. According to the degradation test of RhB under visible light ($\lambda \geq 400$ nm) shown in Fig. 8, photodegradation efficiency (η) of BQDs-BVNFs for RhB reaches 99.6% for 12 min. However, the photodegradation efficiency of BVNFs is only 50% under the same condition.

From the observation of the UV-vis diffuse reflectance spectra and the photocatalytic performance curve diagram, the enhanced activity of the BQDs-BVNFs is not caused by the change in luminous absorption which is blue shift relative to that of BVNFs. Therefore, to figure out the mechanism of action in enhancing photocatalytic performance, the photocurrent transient response measurement of pure BiVO_4 nanofibers and BQDs-BVNFs heterostructure is performed. Fig. 9 shows the rapid and consistent photocurrent responses for BQDs-BVNFs and BVNFs under several on/off visible-light irradiation cycles and electrochemical impedance spectra (EIS) of the two electrodes.

As shown in Fig. 9a, both electrodes are prompt in generating photocurrent with a reproducible response to on/off cycle, indicating the effective charge transfer and successful electron collection for the samples. However, it is worth noting that the BQDs-BVNFs film electrode exhibits an obvious enhanced current density, demonstrating the more efficient photoinduced charge separation and transfer in BQDs-BVNFs. In Fig. 9b, the consequence is further proved by EIS of the electrodes. The arc radius on the Nyquist plot of the BQDs-BVNFs electrode is

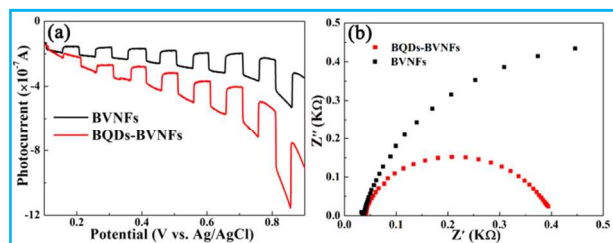


Fig. 9 (a) Photocurrent response of the as-prepared pure BVNFs and BQDs-BVNFs electrodes under visible-light illumination. (b) Electrochemical impedance spectra of BVNFs and BQDs-BVNFs.

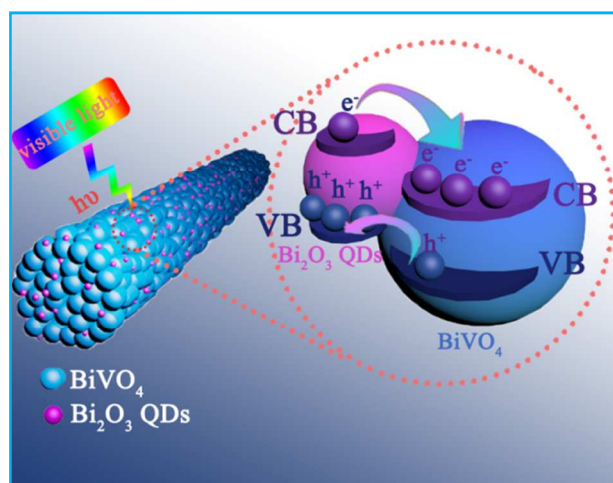


Fig. 10 The mechanism diagram of photocatalysis process.

smaller than that of the BVNFs electrode, which illustrates that the decoration of Bi_2O_3 dots on BiVO_4 nanofibers contribute to a better high-efficiency charge transfer ability. Summing up the above analysis, the enhanced separation and transfer efficiency of the photoinduced carriers may determine the high degradation activity of BQDs-BVNFs.

Subsequently, we proposed the separation process of photoinduced carriers, as shown in Fig. 10. Owing to the formation of Bi_2O_3 QDs surface decoration, it could occur simultaneously that favorable transfer of electrons from Bi_2O_3 to BiVO_4 and holes from BiVO_4 to Bi_2O_3 . As a consequence, the recombination of the photoinduced electron-hole pairs is greatly reduced. Besides, according to the equation $\tau = r^2/\pi^2 D$,⁵³ where τ is the average diffusion time from the bulk to the surface of the photogenerated carriers, r is the grain radius and D is the diffusion coefficient of the carriers, adjusting the particle size to nanoscale can enhance the photocatalytic performance. All the above, owing to the small size of Bi_2O_3 dots, the carriers can transfer to the photocatalysts surface more rapidly and react with the reactants. Therefore, the BQDs-BVNFs could be promising

photocatalysts for photoelectrochemical energy conversion devices.

4. Conclusions

Bi_2O_3 QDs decorated BiVO_4 nanofibers have been *in situ* fabricated by electrospinning based on the phase separation mechanism. The XPS analysis demonstrates that gathering of surface element resulting from the phase separation determines the formation of Bi_2O_3 QDs decoration on BiVO_4 nanofibers. The BQDs-BVNFs exhibits excellent photocatalytic activities on photocatalysis than smooth BiVO_4 nanofibers under visible light irradiation. By investigating the charge transfer property of the two samples, what could be inferred is that the formation of Bi_2O_3 QDs is on account of the improved charge separation and rapid carriers transfer in BQDs-BVNFs. This work not only exploits a facile method for fabrication of high-efficiency QDs decorated photocatalysts but also makes a significant step in fabricating functional material for environment decontamination and practical application.

Acknowledgements

This work was financially supported by the National Nature Science Foundation of China (21271055). We acknowledge for the support by Fundamental Research Funds for the Central Universities (HIT. IBRSEM. A.201410), Open Project of State Key Laboratory of Urban Water Resource and Environment, Harbin Institute of Technology (No. QAK201304) and Program for Innovation Research of Science in Harbin Institute of Technology (B201412).

Notes and references

Department of Chemistry, Harbin Institute of Technology, Harbin, 150001, People's Republic of China. Fax: +86-451-86413753; Tel: +86-451-86413753; E-mail: gchen@hit.edu.cn, jxsun@hit.edu.cn.
† Electronic supplementary information (ESI) available

- X. Wang, J. C. Yu, Y. Chen, L. Wu and X. Fu, *Environ. Sci. Technol.*, 2006, **40**, 2369.
- Z. Zou, J. Ye, K. Sayama and H. Arakawa, *Nature*, 2001, **414**, 625.
- L. Ye, Y. Su, X. Jin, H. Xie and C. Zhang, *Environ. Sci.: Nano*, 2014, **1**, 90.
- H. Cheng, B. Huang and Y. Dai, *Nanoscale*, 2014, **6**, 2009.
- M. Zhang, C. Shao, X. Li, P. Zhang, Y. Sun, C. Su, X. Zhang, J. Ren and Y. Liu, *Nanoscale*, 2012, **4**, 7501.
- M. Zhang, C. Shao, P. Zhang, C. Su, X. Zhang, P. Liang, Y. Sun and Y. Liu, *J. Hazard. Mater.*, 2012, **225**, 155.
- Y. Li, J. Wang, H. Yao, L. Dang, and Z. Li, *Catal. Commun.*, 2011, **12**, 660.
- L. Zhou, W. Wang, S. Sun and M. Shang, *Chem. Eur. J.*, 2009, **15**, 1776.
- D. Hou, W. Luo, Y. Huang, J. C. Yu and X. Hu, *Nanoscale*, 2013, **5**, 2028.
- C. Li, G. Chen, J. Sun, H. Dong, Y. Wang and C. Lv, *Appl. Catal., B*, 2014, **160**, 383.
- M. Shang, W. Wang, J. Ren, S. Sun, L. Wang and L. Zhang, *J. Mater. Chem.*, 2009, **19**, 6213.
- J. Sun, G. Chen, J. Wu, H. Dong and G. Xiong, *Appl. Catal., B*, 2013, **132**, 304.
- A. Walsh, Y. Yan, M. N. Huda, M. M. Al-Jassim and S. Wei, *Chem. Mater.*, 2009, **21**, 547.
- S. Tokunaga, H. Kato and A. Kudo, *Chem. Mater.*, 2001, **13**, 4624.

15. R. Li, F. Zhang, D. Wang, J. Yang, M. Li, J. Zhu, X. Zhou, H. Han and C. Li, *Nat. Commun.*, 2013, **4**, 1432.
16. R. Li, H. Han, F. Zhang, D. Wang and C. Li, *Energy Environ. Sci.*, 2014, **7**, 1369.
17. X. Gao, H. Wu, L. Zheng, Y. Zhong, Y. Hu, and X. (David) Lou, *Angew. Chem.*, 2014, **125**, 6027.
18. M. Shang, W. Wang, J. Ren, S. Sun, and L. Zhang, *CrystEngComm.*, 2010, **12**, 1754.
19. S. Pilli, T. E. Furtak, L. D. Brown, T. G. Deutsch, J. A. Turner and A. M. Herring, *Energy Environ. Sci.*, 2011, **4**, 5028.
20. D. Wang, H. Jiang, X. Zong, Q. Xu, Y. Ma, Dr. G. Li and C. Li, *Chem. Eur. J.*, 2011, **17**, 1275.
21. Z. Wang, C. Yang, T. Lin, H. Yin, P. Chen, D. Wan, F. Xu, F. Huang, J. Lin, X. Xie and M. Jiang, *Adv. Funct. Mater.*, 2013, **23**, 5444.
22. C. Pan, J. Xu, Y. Wang, D. Li and Y. Zhu, *Adv. Funct. Mater.*, 2012, **22**, 1518.
23. S. Cao, Z. Yin, J. Barber, F. Boey, S. Loo and C. Xue, *ACS Appl. Mater. Interfaces*, 2012, **4**, 418.
24. S. Liu, K. Yin, W. Ren, B. Cheng and J. Yu, *J. Mater. Chem.*, 2012, **22**, 17759.
25. W. Sun, Y. Yu, H. Pan, X. Gao, Q. Chen and L. Peng, *J. Am. Chem. Soc.*, 2008, **130**, 1124.
26. D. Liu, Z. Zheng, C. Wang, Y. Yin, S. Liu, B. Yang and Z. Jiang, *J. Phys. Chem. C*, 2013, **117**, 26529.
27. I. Dubé, V. Fabián Ruiz-Ruiz, D. Díaz, S. Posadas and A. Zeinert, *J. Phys. Chem. C*, 2014, **118**, 11495.
28. S. Sun, W. Wang and L. Zhang, *J. Phys. Chem. C*, 2013, **117**, 9113.
29. Y. Dong, C. Chen, X. Zheng, L. Gao, Z. Cui, H. Yang, C. Guo, Y. Chi and C. Li, *J. Mater. Chem.*, 2012, **22**, 8764.
30. D. K. Harris, P. M. Allen, H. S. Han, B. J. Walker, J. Lee and M. G. Bawendi, *J. Am. Chem. Soc.*, 2011, **133**, 4676.
31. H. Li, R. Liu, Y. Liu, H. Huang, H. Yu, H. Ming, S. Lian, S. Lee and Z. Kang, *J. Mater. Chem.*, 2012, **22**, 17470.
32. H. Liu, J. B. Ediel, L. M. Bellan, and H. G. Craighead, *Small*, 2006, **2**, 495.
33. M. Li, J. Zhang, H. Zhang, Y. Liu, C. Wang, X. Xu, Y. Tang and Bai Yang, *Adv. Funct. Mater.*, 2007, **17**, 3650.
34. S. Yang, A. S. Nair, R. Jose and S. Ramakrishna, *Energy Environ. Sci.*, 2010, **3**, 2010.
35. C. J. Luo, S. D. Stoyanov, E. Stride, E. Pelan and M. Edirisinghe, *Chem. Soc. Rev.*, 2012, **41**, 470.
36. C. Zhang and S. Yu, *Chem. Soc. Rev.*, 2014, **43**, 4423.
37. M. Han, T. Sun, P. Tan, X. Chen, O. Tana and M. Tse, *RSC Adv.*, 2013, **3**, 24964.
38. L. Chen, Q. Zhang, R. Huang, S. Yin, S. Luo and C. Au, *Dalton Trans.*, 2012, 41, 9513.
39. J. Zhu, S. Wang, J. Wang, D. Zhang and H. Li, *Appl. Catal., B*, 2011, **102**, 120.
40. J. Hou, Z. Wang, S. Jiao and H. Zhu, *CrystEngComm.*, 2012, **14**, 5923.
41. J. Hou, R. Cao, Z. Wang, S. Jiao and H. Zhu, *J. Hazard. Mater.*, 2012, **177**, 217.
42. P. Zhang, C. Shao, Z. Zhang, M. Zhang, J. Mu, Z. Guo, Y. Sun and Y. Liu, *J. Mater. Chem.*, 2011, **21**, 17746.
43. N. Wang, T. Zhou, J. Wang, H. Yuan and D. Xiao, *Analyst*, 2010, **135**, 2386.
44. D. H. Reneker and I. Chun, *Nanotechnology*, 1996, **7**, 216.
45. J. Yu and A. Kudo, *Adv. Funct. Mater.*, 2006, **16**, 2163.
46. X. Meng, L. Zhang, H. Dai, Z. Zhao, R. Zhang and Y. Liu, *Mater. Chem. Phys.*, 2011, **125**, 59.
47. J. Yu and A. Kudo, *Chem. Lett.*, 2005, **34**, 850.
48. V. Viviera, A. Régis, G. Sagon, J. Y. Nedelec, L.T. Yu and C. Cachet-Vivier, *Electrochim. Acta*, 2001, **46**, 907.
49. J. M. Deitzel, W. Kosik, S. H. McKnight, N. C. Beck Tan, J. M. DeSimone and S. Crette, *Polymer*, 2002, **43**, 1025.
50. P. Dayal and T. Kyu, *J. Appl. Phys.*, 2006, **100**, 043512.
51. R. Kessick and G. Tepper, *J. Appl. Phys.*, 2004, **84**, 4807.
52. C.J. Luo, M. Nangrejo and M. Edirisinghe, *Polymer*, 2010, **51**, 1654.
53. A. Hagfeldt and M. Grätzel, *Chem. Rev.*, 1995, **95**, 49.